Supporting Information

Exemption of Lattice Collapse in Ni-MnO_2 Birnessite Regulated by the Structural Water Mobility

Xiaoqiang Shan,[a] Ranga Teja Pidathala,[b] SaeWon Kim,[a] Wenqian Xu,[c] Milinda Abeykoon,[d] Gihan Kwon,[d] Daniel Olds,[d] Badri Narayanan,[b] and Xiaowei Teng[a*]

[a]Department of Chemical Engineering, University of New Hampshire, Durham, New Hampshire 03824, USA
[b]Department of Mechanical Engineering, University of Louisville, Louisville, Kentucky 40292, USA
[c]Advanced Photon Source, Argonne National Laboratory, Argonne, Illinois 60439, USA
[d]National Synchrotron Light Source II, Brookhaven National Laboratory, Upton, New York 11973, USA

Experimental Sections

Materials synthesis and characterizations: (i) Synthesis of MnO_2; NaOH was ground with 100 mg Mn_3O_4 nanoparticles with the molar ratio of 2:1 using a mortar and pestle. The mixture was then heated in a tube furnace (Thermal Scientific, Inc.) in the open air at 270 °C for 6 hours. The obtained solids were thoroughly washed with DI H_2O and ethanol to remove NaOH residual and vacuum-dried, and then MnO_2 birnessite was obtained. (ii) Synthesis of (Ni)MnO_2; 0.5198 g $MnCl_4{\cdot}4H_2O$ (Alfa Aesar, 99% metals basis) and 0.2246 g $Ni(C_5H_7O_2)_2$ (Alfa Aesar, 95% metal basis) were dissolved in 148.88 mL DI H_2O water with Ni^{2+} and Mn^{2+} atomic ratio 1:3. The solution was magnetically stirred under open-air, and KOH solution (Alfa Aesar, 99.98% metal basis) with a concentration of 0.173 g mL^{-1} was then injected with a rate of 0.167 mL min^{-1} for 50 mins using a programed syringe pump. The obtained precipitate was washed with DI water and ethanol, and then the product was dried and heated at 270 °C for 2 hours in open-air, and finally (Ni)MnO_2 birnessite was obtained. K-ion was chosen in the solution-phase synthesis of (Ni)MnO_2 because it has a smaller hydrated radius (Stokes radius) than Na- and Li-ions, and thus more K-ions could be pre-intercalated in final products. On the other hand, Na-ion was chosen to synthesize MnO_2 birnessite because it has smaller ionic radium than K-ion in a state-state reaction. Notably, both materials were finally thermally treated at 270 °C to ensure the similar crystalline structure and structural water content before characterizations.

Transmission electron microscopy (TEM) images were collected on Zeiss/LEO 922 Omega TEM at the University of New Hampshire. X-ray diffraction was conducted at Beamline 17-BM-B at Advanced Photo Source at the Argonne National Laboratory with a wavelength λ=0.72768 Å, the X-ray scattering measurements were also conducted at 17-BM-B using a wavelength of 0.24116 Å, and the X-ray data were processed with GSAS II software and then analyzed by using PDF gui.[1]

Electrochemical measurements: Cyclic voltammetry (CV) and Chronopotentiometry (CP) measurements of MnO_2 and (Ni)MnO_2 were conducted using a three-electrode half-cell powered by CHI 660d single-channel electrochemical workstation. A glassy carbon rotating disc electrode (Pine Instrument) was used as the working electrode, platinum wire and Ag/AgCl electrode as counter and reference electrodes, respectively. A mixture of 7 mg active material and 3 mg carbon black (Alfa Aesar, >99.9%) was ground and dispersed homogeneously into DI water with a concentration of 1 mg mL^{-1} by sonication. 10 uL suspension containing 7 ug active material and 3 ug carbon black was drop cast onto glassy carbon electrode (0.5 cm in diameter) and vacuum dried. The electrochemical tests were conducted in the 250 mL flask containing 100 mL argon-purged Na_2SO_4 (0.1 M) electrolyte. The CV tests were conducted with an applied potential window from -0.45 V to 1.25 V (vs Ag/AgCl) at the scan rate of 5, 50, 100 and 200 mV s^{-1}. The CP tests were conducted at an applied voltage from -0.45 to 1.25 V (vs Ag/AgCl) at a current density of 1.0 A g^{-1} and also for the same potential range at 2.0 A g^{-1} for 20 cycles.

Ex situ XAS measurements for electrochemical cell: The *ex situ* X-ray absorption spectroscopy (XAS) measurements of MnO_2 and (Ni)MnO_2 birnessite were conducted right after charging at Beamline 6-BM at NSLS-II Brookhaven National Laboratory. The electrodes were prepared by deposited the mixture of 90 % active material and 10 % carbon black on thin Tray carbon paper

and were cycled at 5 mV s^{-1} using CV and then charged to 1.25 V (vs Ag/AgCl) at 0.5 mV s^{-1} and afterward hold at 1.25 V for 10 minutes. The electrodes were washed with DI H_2O to remove the salts. The dried electrode is sealed by Kapton tape and then characterized with XAS. The XAS data were analyzed by using ATHENA software.

In situ XRD characterizations for electrochemical cell: In situ XRD test of MnO_2 in a home-made electrochemical cell at beamline 17-BM-B using a wavelength of 0.72768 Å and *in situ* XRD test of (Ni)MnO_2 were conducted in a similar cell at beamline 28-ID-1 at Brookhaven National Laboratory with a wavelength of 0.166 Å. The mixture of 90 % active material and 10 % carbon black was deposited on the thin carbon paper and dried naturally in an open-air as the working electrode. The platinum wire and micro Ag/AgCl electrode as counter and reference electrode, respectively, and 0.5 M Na_2SO_4 electrolyte was used as electrolyte. Electrochemical CV testing was applied at a scan rate of 1 mV s^{-1} for 2 cycles, and the XRD was collected during the CV scans. *In situ* XRD results were analyzed by using GSAS II software.

First-principles calculations: All the first-principles calculations were performed within the framework of Hubbard-corrected density functional theory (DFT+*U*) using the projected-augmented plane wave method as implemented in Vienna *Ab initio* Simulation Package (VASP).[2-3] We described the exchange correlations using the Perdew–Burke–Ernzerhof (PBE) functionals[4] within the generalized gradient approximation using the pseudopotentials supplied by VASP: Mn_pv (valence: $3d^5\ 4s^2$), O (valence: $2s^2\ 2p^4$), Na_pv (valence: $3s^1$), H (valence: $1s^1$) and Ni_pv (valence: $3d^8\ 4s^2$). Hubbard correction was employed to treat electron localization on Ni and Mn atoms using a rotationally-invariant form of DFT + *U* formulated by Liechtenstein *et al.*[5] with U = 4.6 eV and J = 0.6 eV following previous works on birnessite.[6] The computational supercell consisted of 3 × 1 × 1 unit cells of layered δ–MnO_2 with one Na and 9 H_2O molecules in the interlayer region (resulting in $NaMn_6O_{12}.9H_2O$). Note that birnessite can contain up to 3 Na for this composition;[7] we used only one Na to simulate the Na-lean conditions typically encountered during deep charge. We employed a plane wave energy cutoff of 540eV and 4×3×2 Monkhorst-Pack grid to sample the Brillouin zone. All the atomic coordinates, including the lattice parameters, were relaxed in MnO_2 and (Ni)MnO_2 using gaussian smearing with a smearing width of 0.05 eV until the force on each atom was lower than 0.005 eV/Å. The atomic charges were calculated using Bader analysis on the charge density grids for the relaxed structures.

Classical molecular dynamics simulations: All the classical molecular dynamics simulations were performed with a popular open-source package LAMMPS.[8] The computational supercell (dimensions: a = 70.6078Å, b = 13.4598 Å, c = 33.1434Å, α = 92.5°, β = 102.6° and γ = 89.9°) consisted of 12 × 4 × 4 unit cells of layered δ–MnO_2 with 64 Na, and 320 structural water in the interlayer region (resulting in $Na_{64}Mn_{384}O_{768}.320H_2O$). The initial configurations for different Ni locations were constructed by replicating the equilibrium structures derived from DFT along the periodic directions. We modeled the atomic interaction in the (Ni)MnO_2 birnessite lattice using a general force field, CLAYFF, developed by Cygan *et al* [9]with Lennard Jones force-field parameters taken from earlier work by Newton and Kwon.[10] The structural water was described using SPC/E model,[11] and interactions involving Na^+ ions were accounted using Lennard-Jones potential.[10] The atomic charges were set at values obtained from Bader analysis of equilibrium structures derived from DFT. Long-range Coulombic interactions were accounted using the particle-meh Ewald method as implemented in LAMMPS. Previous CMD studies have shown that

this approach provides excellent description of structure, thermodynamics, ion-solvation behavior, and transport properties of MnO_2 birnessite.[9, 12]

CMD simulations were performed within the isobaric – isothermal ensemble (NPT) under ambient conditions for 5 ns, with a timestep of 0.5 fs. Constant pressure and temperature conditions were maintained using Nose-Hover thermostat/barostat. SHAKE algorithm[13-14] implemented within LAMMPS was used to constraint angles and bonds of the water molecules (as required for SPC/E model). Diffusivity of structural water and Na were calculated using the temporal evolution of mean-squared displacement of desired species averaged over last 4 ns of CMD trajectories.

Supplementary Figures:

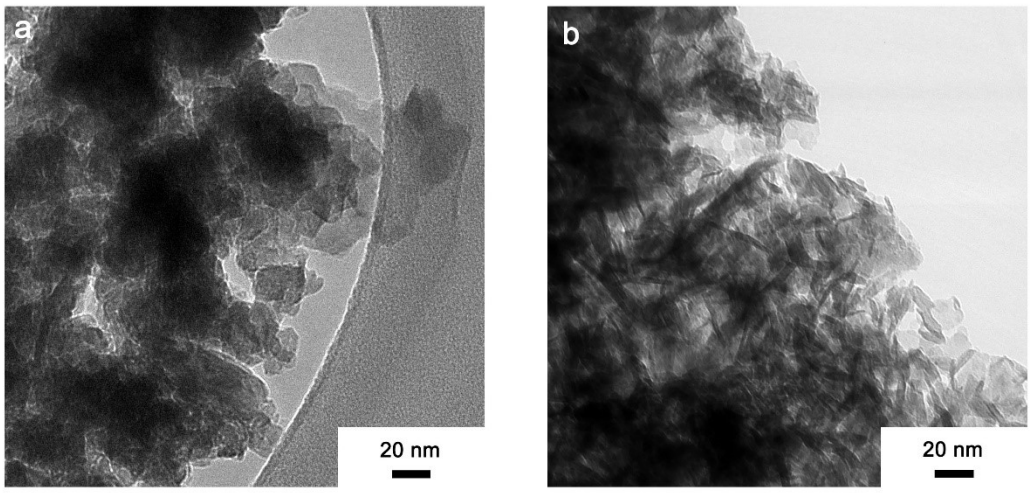

Figure S1. TEM images of (a) MnO_2 and (b) (Ni)MnO_2.

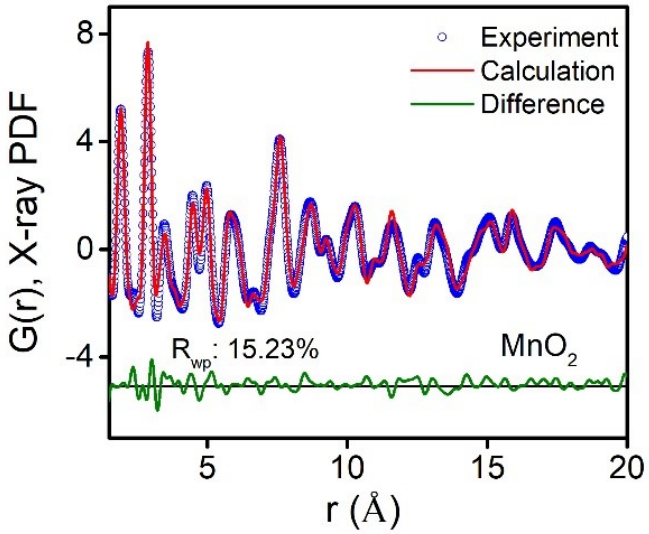

Figure S2. X-ray PDF analysis of MnO_2.

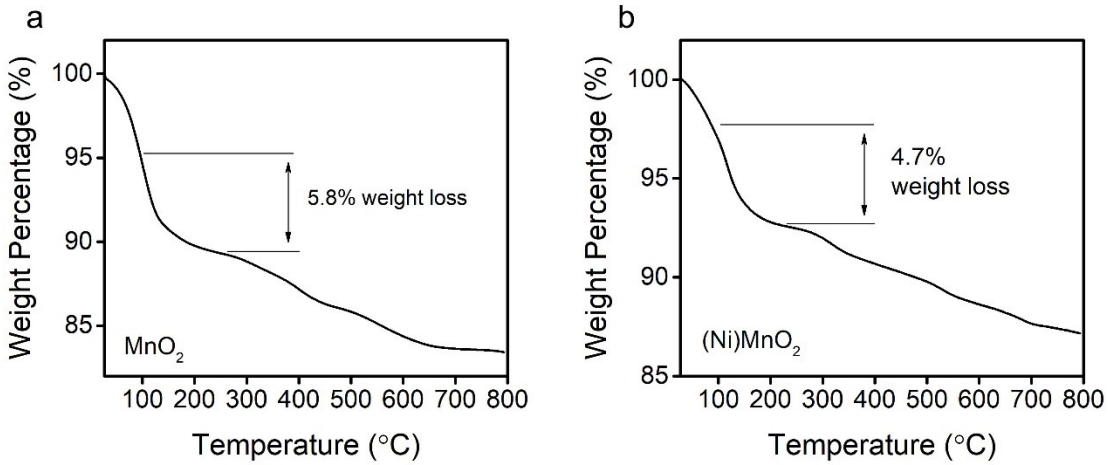

Figure S3. TGA of MnO_2 and (Ni)MnO_2.

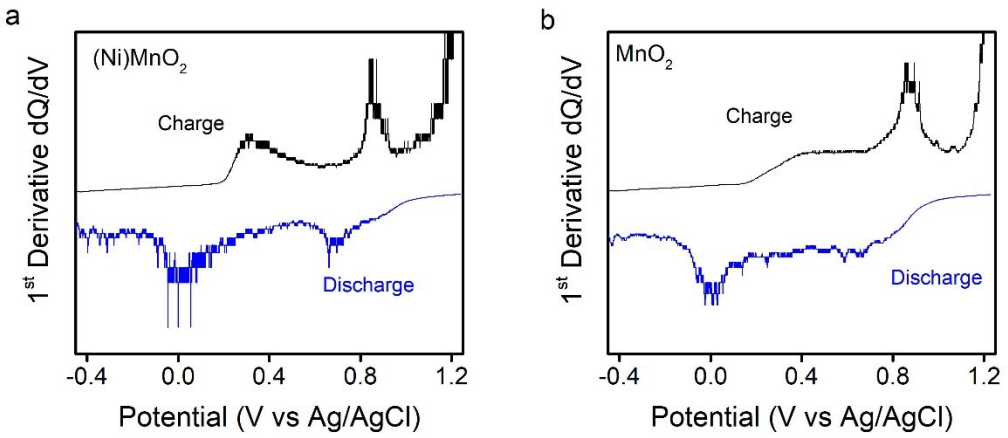

Figure S4: The dQ/dV (1st order derivative of charge with respective to potential) plots obtained from CP measurements of (a) (Ni)MnO_2 and (b) MnO_2 materials.

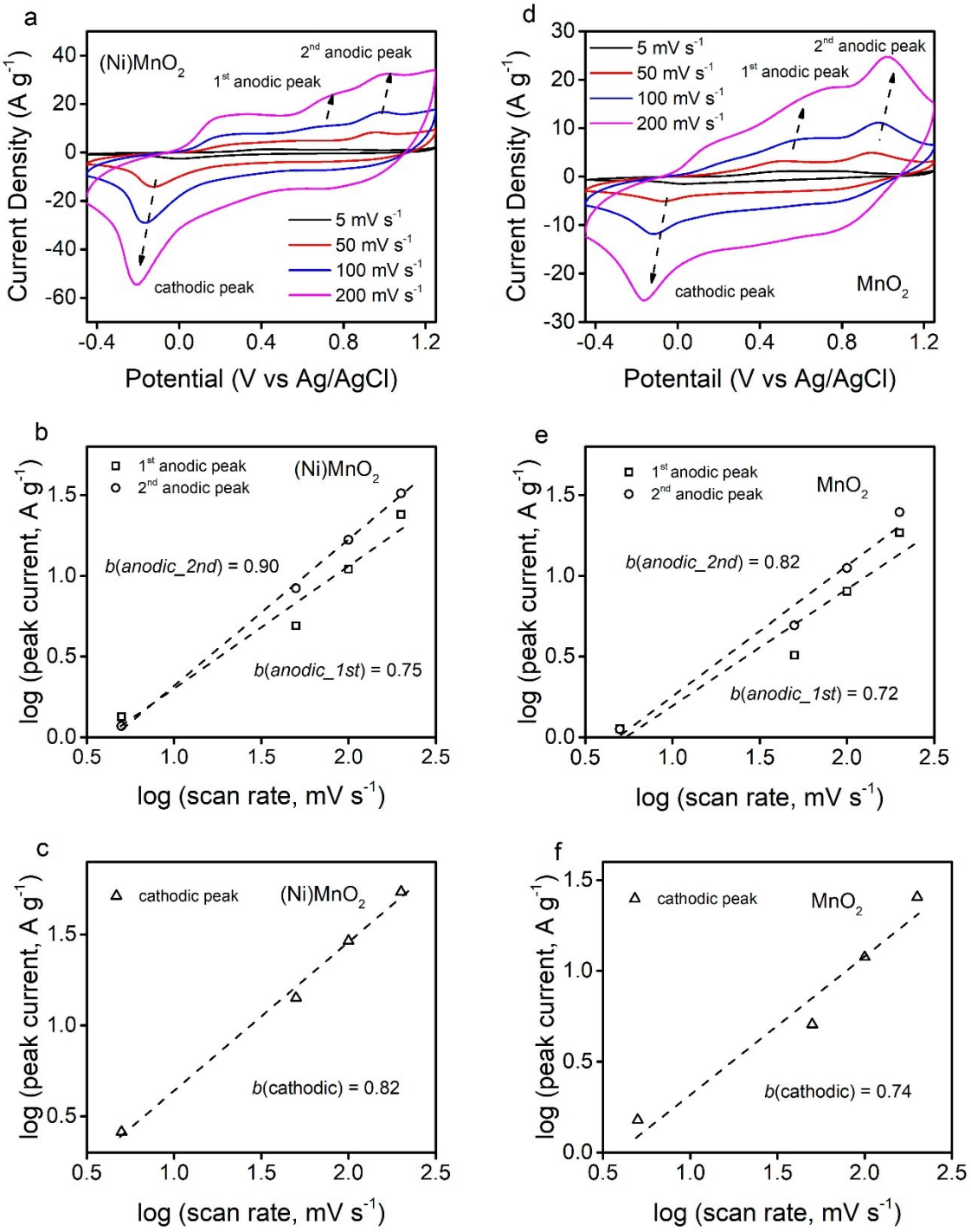

Figure S5. (a,d) CVs of (Ni)MnO_2 and MnO_2 at the scan rates from 5 to 200 mV s^{-1}; (b,e) *b*-values of anodic peaks; (c,f) *b*-values of cathodic peaks.

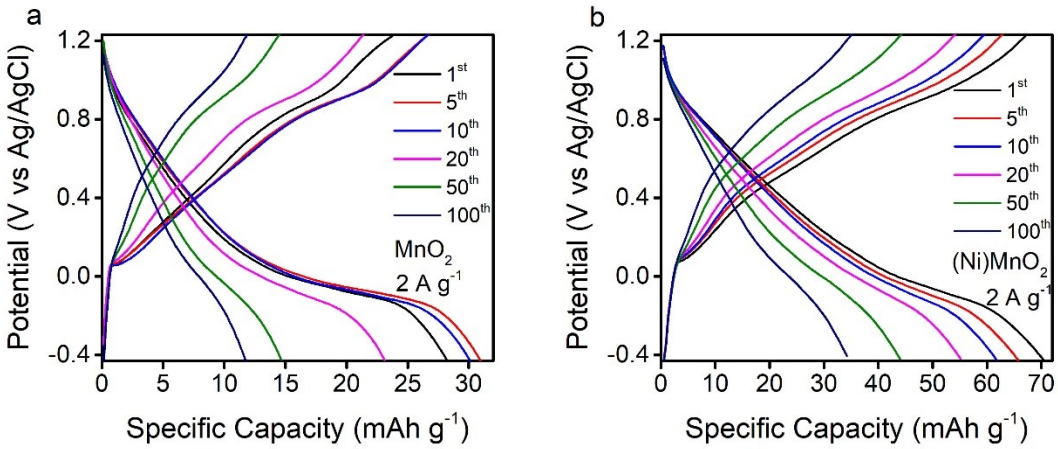

Figure S6. Charge and discharge profiles of MnO_2 and (Ni)MnO_2 at 2 A g^{-1} with plotted 1st, 5th, 10th, 20th, 50 th, and 100 th cycles.

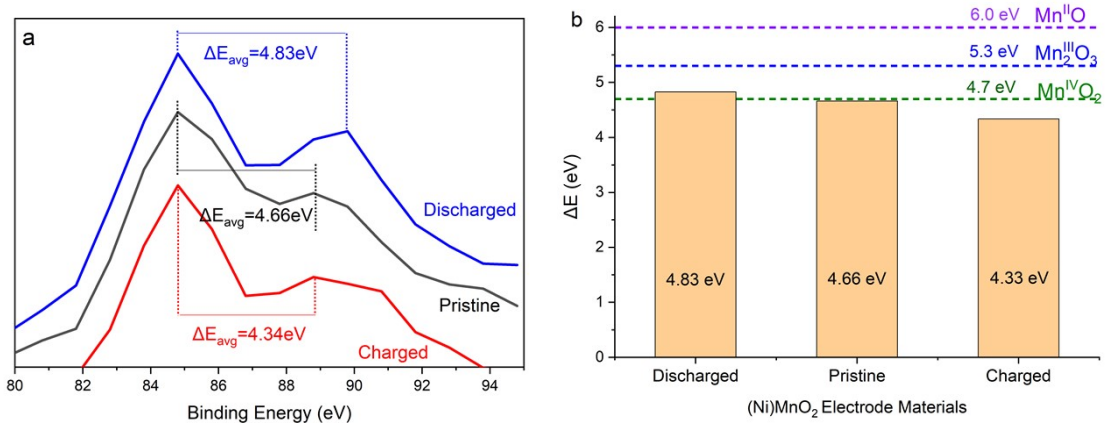

Figure S7 (a) XPS Mn 3s spectra of pristine, discharged (-0.45 V vs. Ag/AgCl), and charged (1.25 V vs. Ag/AgCl) (Ni)MnO_2 electrode materials; (b) Mn 3s multiplet split of (Ni)MnO_2 in different electrochemical states, in comparison with the split from MnO, Mn_2O_3, MnO_2 standards.

Supplementary Tables:

Refined crystal structural parameters of MnO_2

Atom	Type	x	y	z	Occ.	Site	Uiso	U_{11}	U_{22}	U_{33}	U_{13}
Mn1	Mn+4	0	0	0	1.00	1a	0.05	0.012	0.010	0.122	0.005
Mn2	Mn+4	0.500	0.500	0	1.00	1e	0.05	0.012	0.010	0.122	0.005
O1	O-2	0.620	0.001	0.863	1.00	2i	0.03	0.044	0.008	0.025	0.006
O2	O-2	0.120	0.501	0.863	1.00	2i	0.03	0.044	0.008	0.025	0.006
Na1	Na+1	0.452	0.803	0.467	0.145	2i	0.13	0.025	0.020	0.366	0.044
Na1	Na+1	0.952	0.303	0.467	0.145	2i	0.13	0.025	0.020	0.336	0.044
O3	O-2	0.452	0.803	0.467	0.478	2i	0.13	0.025	0.020	0.336	0.044
O4	O-2	0.952	0.303	0.467	0.478	2i	0.13	0.025	0.020	0.336	0.044

Space group: P-1

a=5.044 b=2.868 c=7.281(Å) α=88.848 β=100.119 γ=88.969 (°)

Table S1. Refined crystal structural parameters of MnO_2 material with X-ray PDF fitting up to 20 Å with R_{wp}=15.23%. The sodium and water amount were determined from EDXS and TGA measurements.

Refined crystal structural parameters of (Ni)MnO_2

Atom	Type	x	y	z	Occ.	Site	Uiso	U_{11}	U_{22}	U_{33}	U_{13}
Mn1	Mn+4	0	0	0	0.77	2a	0.04	0.004	0.010	0.108	0.013
Ni1	Ni+2	0	0	0	0.23	2a	0.14	0.005	0.013	0.393	0.023
O1	O-2	0.343	0	0.148	1.00	4i	0.01	0.013	0.006	0.004	0.008
O2	O-2	0.380	0	0.443	0.66	4i	0.07	0.007	0.187	0001	0.004
K1	K+1	0.380	0	0.442	0.06	4i	0.07	0.007	0.187	0.001	0.004
O3	O-2	0	0	0.500	0.20	2c	0.02	0.008	0.063	0.018	0.057

Space group: C 2/m

a=4.954 b=2.896 c=7.069 (Å) α=90 β=95.665 γ=90 (°)

Table S2. Refined crystal structural parameters of (Ni)MnO_2 material with X-ray PDF fitting up to 15 Å with R_{wp}=20.33%. The potassium and water amount were determined from EDXS and TGA measurements.

Number	Electrode Materials	Capacity (mAh g^{-1})	Retention (cycles)	Reference
1	δ-(Ni)MnO_2	96 @1Ag^{-1}	49.6% (100) @2Ag^{-1}	Our work
2	δ-MnO_2	47 @1Ag^{-1}	41.7% (100) @2Ag^{-1}	Our work
3	δ-H-MnO_2	~90 @ 2C	~66% (500) @2C	Ref. 15
4	$Al_{0.05}Mn_{0.95}O_2$	20 @ 0.2Ag^{-1}	74% (500) @ 0.2Ag^{-1}	Ref. 16
5	$Na_{0.75}Ni_{0.82}Co_{0.12}Mn_{0.06}O_2$	80 @1C	65% (300) @1C	Ref. 17

Table S3: The comparison of electrochemical performance between the reported MnO_2-based electrode materials and the ones reported in this study.

Ni substituted at various Mn Octahedral sites	Energy (eV/atom)	Interplanar spacing (Å)
MnO_2	-6.1195	7.3703
(Ni)MnO_2 Site I	-5.9317	7.3485
(Ni)MnO_2 Site II	-5.9319	7.3478
(Ni)MnO_2 Site III	-5.9364	7.3903
(Ni)MnO_2 Site IV	-5.9352	7.3322
(Ni)MnO_2 Site V	-5.9483	7.4833
(Ni)MnO_2 Site VI	-5.9348	7.3274

Table S4: Effect of location of Ni dopant on the cohesive energy (eV/atom) and interlayer spacing (Å) for $Na_{0.17}Ni_{0.17}Mn_{0.83}O_2.0.8333H_2O$ in the deep charging case. The location of Ni is marked by I to VI in Figure 4 of the main text.

Reference:

1. Toby, B. H.; Von Dreele, R. B., GSAS-II: the genesis of a modern open-source all purpose crystallography software package. *Journal of Applied Crystallography* **2013,** *46* (2), 544-549.
2. Kresse, G.; Furthmüller, J., Efficient iterative schemes for ab initio total-energy calculations using a plane-wave basis set. *Physical Review B* **1996,** *54* (16), 11169-11186.
3. Kresse, G.; Joubert, D., From ultrasoft pseudopotentials to the projector augmented-wave method. *Physical Review B* **1999,** *59* (3), 1758-1775.
4. Perdew, J. P.; Burke, K.; Ernzerhof, M., Generalized Gradient Approximation Made Simple. *Physical review letters* **1996,** *77* (18), 3865-3868.
5. Liechtenstein, A. I.; Anisimov, V. I.; Zaanen, J., Density-functional theory and strong interactions: Orbital ordering in Mott-Hubbard insulators. *Physical Review B* **1995,** *52* (8), R5467-R5470.
6. Tompsett, D. A.; Parker, S. C.; Islam, M. S., Surface properties of α-MnO2: relevance to catalytic and supercapacitor behaviour. *Journal of Materials Chemistry A* **2014,** *2* (37), 15509-15518.
7. Lucht, K. P.; Mendoza-Cortes, J. L., Birnessite: A Layered Manganese Oxide To Capture Sunlight for Water-Splitting Catalysis. *The Journal of Physical Chemistry C* **2015,** *119* (40), 22838-22846.
8. Plimpton, S., Fast Parallel Algorithms for Short-Range Molecular Dynamics. *Journal of Computational Physics* **1995,** *117* (1), 1-19.
9. Cygan, R. T.; Liang, J.-J.; Kalinichev, A. G., Molecular Models of Hydroxide, Oxyhydroxide, and Clay Phases and the Development of a General Force Field. *The Journal of Physical Chemistry B* **2004,** *108* (4), 1255-1266.
10. Newton, A. G.; Kwon, K. D., Molecular simulations of hydrated phyllomanganates. *Geochimica et Cosmochimica Acta* **2018,** *235*, 208-223.
11. Berendsen, H. J. C.; Grigera, J. R.; Straatsma, T. P., The missing term in effective pair potentials. *The Journal of Physical Chemistry* **1987,** *91* (24), 6269-6271.
12. Cheng, W.; Lindholm, J.; Holmboe, M.; Luong, N. T.; Shchukarev, A.; Ilton, E. S.; Hanna, K.; Boily, J.-F., Nanoscale Hydration in Layered Manganese Oxides. *Langmuir* **2021,** *37* (2), 666-674.
13. Ryckaert, J.-P.; Ciccotti, G.; Berendsen, H. J. C., Numerical integration of the cartesian equations of motion of a system with constraints: molecular dynamics of n-alkanes. *Journal of Computational Physics* **1977,** *23* (3), 327-341.
14. Andersen, H. C., Rattle: A "velocity" version of the shake algorithm for molecular dynamics calculations. *Journal of Computational Physics* **1983,** *52* (1), 24-34.
15. Thapa, A. K.; Pandit, B.; Thapa, R.; Luitel, T.; Paudel, H. S.; Sumanasekera, G.; Sunkara, M. K.; Gunawardhana, N.; Ishihara, T.; Yoshio, M., Synthesis of mesoporous birnessite-MnO2 composite as a cathode electrode for lithium battery. *Electrochimica Acta* **2014,** *116*, 188-193.
16. Li, Y.; Xie, H., Mechanochemical-synthesized Al-doped manganese dioxides for electrochemical supercapacitors. *Ionics* **2010,** *16* (1), 21-25.
17. Yang, J.; Tang, M.; Liu, H.; Chen, X.; Xu, Z.; Huang, J.; Su, Q.; Xia, Y., O3-Type Layered Ni-Rich Oxide: A High-Capacity and Superior-Rate Cathode for Sodium-Ion Batteries. *Small* **2019,** *15* (52), 1905311.